Inorganic Chemistry

Article

pubs.acs.org/IC

Magnetic Anisotropy and Mechanism of Magnetic Relaxation in Er(III) Single-Ion Magnets

Saurabh Kumar Singh, Tulika Gupta, and Gopalan Rajaraman*

Department of Chemistry, Indian Institute of Technology−Bombay, Mumbai 400076, India

Supporting Information

ABSTRACT: Magnetic anisotropy is a key component in the design of single-molecule magnets (SMMs) possessing a large barrier height for magnetization reversal. Lanthanide-based SMMs are the most promising candidates in this arena as they offer a large magnetic anisotropy due to the presence of strong spin−orbit coupling. Among lanthanides, Er(III) complexes are gaining attention in the area of SMMs, because of their intriguing magnetic properties and attractive blocking temperatures. Here, we have undertaken detailed *ab initio* calculations on four structurally diverse Er(III) SMMs to shed light on how the magnetic anisotropy is influenced by the role of symmetry and structural distortions. The employed CASSCF+RASSI calculations have offered rationale for the observed differences in the estimated U_{eff} values for the studied complexes and also offered hints to the mechanism of magnetic relaxation. The differences in the mechanism of magnetic relaxations are further analyzed based on the Er−ligand interactions, which is obtained by analyzing the charges, densities, luminescent behavior and the frontier molecular orbitals. Our calculations, for the first time, have highlighted the importance of high symmetry environment and ligand donor strength in obtaining large U_{eff} values for the Er(III) complexes. We have examined these possibilities by modeling several structures with variable coordination numbers and point group symmetry. These results signify the need of a detailed understanding on the shape of the anisotropy and the point group symmetry in order to achieve large U_{eff} values in Er(III) single-ion magnets.

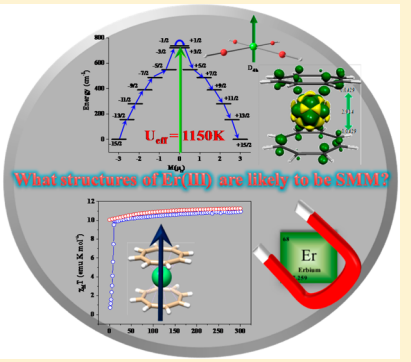

1. INTRODUCTION

After the discovery of the first single-ion magnet $[TbPc_2]^-$ (where Pc_2^- = pthalocyanine dianion),[1] lanthanide based complexes have gained momentum in the area of molecular magnetism as they exhibit slow relaxation of magnetization at low temperatures.[1,2] Thanks to their unquenched orbital angular momentum and inherent magnetic anisotropy, the number of lanthanide-based single-molecule magnets (SMMs) reported to-date is increasing exponentially.[2e,f,3] Beyond fundamental interest, these molecules are also proposed to have great deal of potential applications ranging from highly dense information storage devices, Q-bits in quantum computing, to spintronics devices.[2b−d,4]

Despite tremendous efforts on the synthesis of polynuclear SMMs based on lanthanides, the SMM characteristics of many polynuclear SMMs are single ion in origin.[3e,5] An example that illustrates this category is the report of $\{Dy_5\}$ cluster exhibiting a barrier height (U_{eff}) of 800 K, which originates from a single Dy(III) ion.[6] The presence of strong exchange-coupling between lanthanides and transition metals[3d,7] or radicals[8] generally leads to superior SMMs. Elegant examples to this category are the reports of $\{Dy_2Cr_2\}$ SMM and $\{TbN_2^{3-}\}$ complexes,[7b,8d,e] showing blocking temperatures of 3.7 and 14 K, respectively.

The future success in the synthesis of new- generation lanthanide SMMs relies heavily on a perceivable approach to obtain symmetric structures and ways to control the quantum tunnelling of magnetization (QTM), which diminishes the SMM behavior. In this regard, numerous mononuclear single-ion magnets (SIMs) have been synthesized to gain clear understanding on the QTM effects and the magnetic relaxation phenomena. The most prolific example in this category is the anisotropic Dy(III) ion, which holds the maximum number of SMMs reported in the lanthanide series.[2g,3b,d,5a,c,d,7a−c,g,8c,9] Lanthanide complexes possessing a half-integer ground state (Kramers ions), are considered superior to non-Kramers ions for the SMM behavior, and, thus, they are natural target for the synthetic chemists.[10] Apart from the choice of the metal ions, the ligand design also plays an important role, as illustrated in the case of $[TbPc_2]^-$, where a high-symmetry environment leads to a large barrier height, even for a non-Kramers Tb(III) ion. Recently, Long et al.[3e] reported a detailed description of achieving large magnetic anisotropy in lanthanide-based complexes and explored the importance of crystal field environment in the lanthanide series. The elaborated concept based on ligand field theory highlights the importance of the ligand field environment (prolate/oblate shape[11] of electron cloud) in achieving larger U_{eff} values. Besides, the lanthanide SMMs also exhibit exquisite properties, such as luminescence, when they combine with the apt ligands and this feature expands its potential applications to other territories.[9a,12]

Received: April 3, 2014
Published: September 26, 2014

One of the challenging tasks in the area of lanthanides is to find a way to characterize and understand the Stark levels.[13] Over the years, Chibotaru et al.[3d,5b,6,7b,9d,g,10,14,48,49] have developed and employed the rigorous *ab initio* calculations to shed light on this issue. In addition, they have offered a pseudo-spin Hamiltonian approach to access the energies of Stark levels and the associated anisotropy. This method has now been adapted by several groups to verify the observed magnetic properties[2e,9e,l,m,7c,15] and has also been proved useful to validate the magnetic anisotropy data obtained from EPR measurement.[9m,10,16,10,16e,17d,18] The majority of the lanthanide-based SMMs reported to date contain oblate ions, such as Dy(III), Tb(III), and Ho(III), while SMMs based on prolate ions are rather limited in number. The Er(III) complexes are the only ones known in the prolate series to exhibit SMM characteristics.[17,18] This is rather intriguing as both type of the ions, subject to the ligand design, have equal probability to exhibit SMM characteristics.

Although strong L+S coupling has been advocated to rationalize the preferred choice of the ions, the prolate type ions such as Er(III) also possess strong L+S coupling, but the observation of SMM characteristics in these ions is rather scarce.[17b−g,18] Recently, Pablo et al.[19] reported a mononuclear Er(III) complex possessing a square antiprismatic coordination environment with tris(2,2,6,6-tetramethyl-3,5-heptanedionato) and mono (bathophenanthroline) ligands. This complex exhibits slow relaxation of magnetization with a U_{eff} value of 22.4 K in the presence of an applied external magnetic field of 0.05 T (field-induced SMM,[20] fSMM). This complex also shows luminescent properties in the near-infrared (NIR) region. On the other hand, Gao et al. have reported a Er(III) complex $[Er(acac)_3(H_2O)_2]$ that also possesses a square antiprismatic coordination environment, but does not show any SMM characteristics.[5d,9k,21] An elegant addition to this array is the [ErCp*(COT)] complex, which is a natural SMM (nSMM) with a blocking temperature (T_B) of ∼5 K.[22,23] In a similar context, Long et al. have recently reported a mononuclear highly symmetric $[Er(COT)_2]^-$ complex,[17f] and this is, again, a nSMM with a U_{eff} value of 216 K and possesses the second-largest T_B value reported for any SMMs (10 K). This is followed by a report of another complex, $[Er(COT'')_2]^-$, which has trimethylsilyl ($SiMe_3$) substituents at the 1,4 positions and this is also a nSMM with U_{eff} = 187 K and T_B = 8 K.[17c]

The lack of SMM behavior in the majority of the Er(III) complexes and the presence of large T_B values in some other Er(III) complexes have attracted our attention. This illustrates that ligand field design plays a crucial role for the observance of SMM behavior in Er(III) complexes. To resolve some of the intriguing questions in this area, here, we have modeled four Er(III) complexes: $[Er(thd)_3(bath)]$, where thd = (2,2,6,6-tetramethyl-3,5-heptanedionate) and bath = bathophenanthroline (**1**); $[Er(COT)_2]^-$, where COT= (cyclooctatetraenyl dianion) (**2**); $[Er(COT'')_2]^-$, where COT″ = 1,4-bis-(trimethylsilyl) cyclooctatetraenyl dianion (**3**), and [Er(COT)-Cp*]$^-$, where Cp* = pentamethylcyclopentadienide and COT = cyclooctatetraenyl dianion (**4**). By modeling these four structures, our objective is to answer the following intriguing questions:

(i) What are the origin of magnetic anisotropy and the mechanism of magnetization relaxation in these SMMs?
(ii) Why is one of them a field-induced SMM while the others are zero-field SMMs?
(iii) What is the role of geometry and coordination number, with regard to the U_{eff} values?

2. COMPUTATIONAL DETAILS

Here, we have performed all the *ab initio* calculations using MOLCAS 7.8 suite.[24] We have employed the [ANO-RCC[25]...7s6p4d2f1g.] basis set for Er atoms, the [ANO-RCC...3s2p.] basis set for C atoms, the [ANO-RCC...2s.] basis set for H atoms, the [ANO-RCC...3s2p1d.] basis set for N atoms, the [ANO-RCC...4s3p.] basis set for Si atoms, and the [ANO-RCC...3s2p1d.] basis set for O atoms. The ground-state f-electron configuration for Er(III) is 4f,[11] and this yields a $^4I_{15/2}$ multiplet as the ground state. First, we have performed CASSCF[26] calculations with an active space of 11 active electrons in seven 4f orbitals (11,7). With this active space, we have computed 35 quartets as well 112 doublet states in the Configuration Interaction (CI) procedure. After computing these excited states, we have mixed all 35 of these quartets and all 112 of these doublets using RASSI-SO[26] module to compute the spin−orbit coupled states. Furthermore, we have taken these computed SO states into the SINGLE_ANISO[27] program to compute the *g*-tensors. The Er(III) ion has eight low-lying Kramers doublets for which the anisotropic g-tensors have been computed. The Cholesky decomposition for two electron integrals is employed throughout our calculations. Using the SINGLE_ANISO code, we have also extracted the crystal field parameters as implemented in MOLCAS 7.8. The transition matrix elements are computed using a MOLCAS routine provided by Prof. L. Chibotaru (University of Leuven, Belgium).[28] There are several reports on Er(III) complexes that utilize the same methodology as the one above, although there are some reports that emphasize the importance of dynamic correlation to improve the description of magnetic anisotropy.[26,47] Structural optimization, Mulliken charges, and the spin densities have been computed using DFT calculations employing the Gaussian 09[29] suite. Here, we have employed the B3LYP[30] functional, along with the Cundari−Stevens double-ζ polarization basis set,[31] for the Er(III) ions and the Ahlrichs triple-ζ basis set[32] has been employed for the rest of the atoms. Absorption spectrum has been computed using time-dependent density functional (TD-DFT) theory,[33] as implemented in ORCA[34] software suite. These calculations also employ B3LYP functional along with the Ahlrichs triple-ζ basis set[32] for all of the lighter elements. This calculation has been performed incorporating solvation effects using Continuum Super Conductor Model (COSMO) solvation model[35] and employing methanol as the solvent.

3. RESULTS AND DISCUSSION

Here, we have chosen four structures for our study: these are labeled as complexes **1**−**4**. Complex **1** consists of eight coordinate Er(III) in square antiprismatic coordinating environment, composed of six O atoms from the three −thd ligands and two N atoms from the −bath ligand (see Figure 1a). On the other hand, the **2**−**4** sandwich complexes comprise COT ligands where essentially the aromatic π orbitals are coordinating to the metal ion. Complex **2** specifically has a C_8 principal axis of symmetry with the point group close to that of D_{8h} (see Figure 1b). Complex **3** is structurally similar to **2** and it possesses two trimethylsilyl ($SiMe_3$) substituent at the 1,4 positions of the COT ligands, which destroys the C_8-axis (see Figure 1c). Complex **4** is also based on the COT ligand, but it additionally possesses a Cp* ligand *trans* to COT (see Figure 1d). Before we begin our discussion on the computed magnetic anisotropy, we would like to ascertain confidence on the computed parameters by simulating the magnetic susceptibility for complexes **1**−**4**, using CASSCF energies. Although minor variations are visible (see Figure 2), generally,

dx.doi.org/10.1021/ic500772f | Inorg. Chem. 2014, 53, 10835−10845

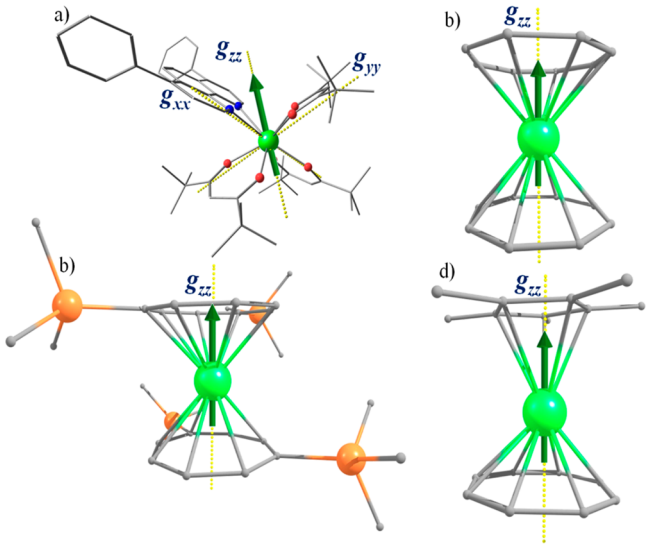

Figure 1. *Ab initio* computed orientation of *g*-tensors of the ground-state KDs for complexes (a) **1**, (b) **2**, (c) **3**, and (d) **4**. Color scheme: green, Er; orange, Si; blue, N; red, O; and black, C. All the hydrogen atoms are omitted for the sake of clarity.

the computed susceptibility reproduces the experimental data, particularly both the shapes and minor differences in the room-temperature $\chi_m T$ values among complexes **1**−**4** are nicely reproduced.

For complex **1**, the computed ground-state anisotropies are g_{xx} = 0.6742, g_{yy} = 1.4119, and g_{zz} = 14.8817; this is a rather axial set of anisotropy and lacks pure Ising nature (see Table 1 and Table S2 in the Supporting Information for details). All the eight Kramers doublets (KDs) are found to span over an energy window of 325 cm^{-1}. The relative energies of the eight low-lying KDs, along with the computed anisotropy, are given in Table 1 (also see Tables S1 and S2 and Figure S1 in the Supporting Information). The computed g_{zz} orientation for the ground-state KD in **1** is found to be directed toward one of the −N donors of bathophenanthroline ligand and is tilted 25.8° from the Er−N bond vector (see Figure 1a). The orientation of the g_{zz} vector in this case is not surprising, since it has chosen to align with the ligand possessing the least electrostatic repulsion.

Table 1. *Ab Initio* Computed Principal Values of Ground-State *g*-Tensors for All Four Complexes, along with the Computed Barrier Height for Magnetization Reversal

	1	2	3	4
g_{xx}	0.6742	0.0000	0.0000	0.0004
g_{yy}	1.4119	0.0000	0.0000	0.0009
g_{zz}	14.8817	17.9439	17.9413	17.9214
ΔE (cm^{-1})	37.0	280.4[a]	247.1[a]	164.5

[a]In these cases, the barrier heights are calculated between the ground state and the second excited state, because the principal magnetization axes of the ground start and first excited KDs are found to be collinear.

Since all the oxygen atoms carry a formal negative charge, the Er−N bond direction is preferred for the g_{zz} vector orientation. The computed NPA charges illustrate the above points that all the oxygen atoms are found to possess an average negative charge of −0.32 while nitrogen atoms possess an average negative charge of −0.18 (see Table S3 in the Supporting Information). Orientation of magnetic anisotropy as well as magnetic moment computed has been found to minimize the electrostatic energy (i.e., electrostatic repulsion between ligands and electron density of the metals).[36]

To probe the mechanism of relaxation, data beyond the ground-state KDs must be analyzed. The magnetic relaxation in lanthanides is found to occur essentially because of three factors, in the absence of intermolecular interactions:[5b,37]

(i) via QTM between the ground-state KDs, which occurs due to large transverse anisotropy of the ground-state KDs;
(ii) via the Orbach/Raman process[38] which accounts for the relaxation via the excited KDs and occurs essentially due to the noncoincidence of the principal anisotropic axes; and
(iii) via thermally assisted QTM (TA-QTM), which accounts for relaxation via the excited states due to the non-Ising nature of the excited KDs.

Qualitative mechanism of relaxation obtained from *ab initio* calculations for **1** is shown in Figure 3a. Here, the states are arranged according to the values of their magnetic moments. The number at each arrow connecting any two states is the

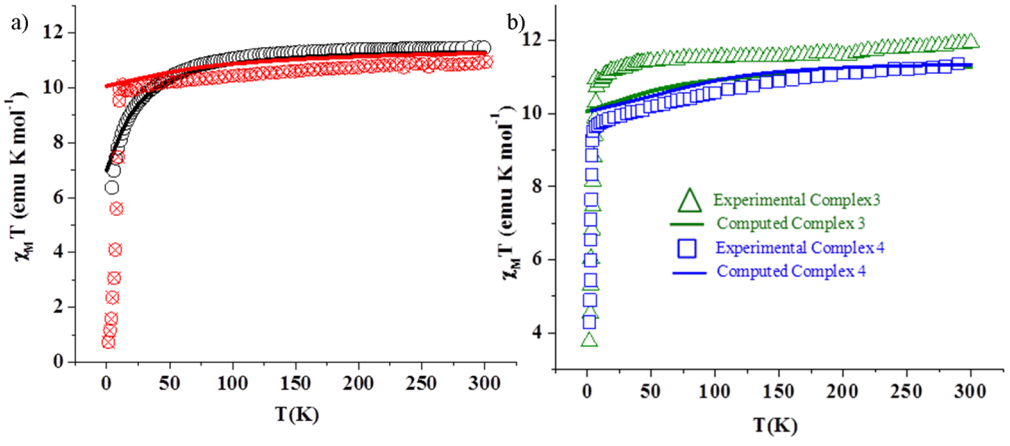

Figure 2. Experimental and *ab initio* computed molar magnetic susceptibility plots for complexes (a) **1** and **2** and (b) **3** and **4**. The black hollow circles, red hollow crossed circles, green hollow triangles, and blue hollow squares are the experimental magnetic susceptibility for complexes **1**−**4**, respectively, extracted from the experimental plots.[17c,f,19,22] The solid lines corresponding to the same color code are the *ab initio* computed molar magnetic susceptibilities. Note the intermolecular interaction *zJ* is taken as zero in these calculations.

dx.doi.org/10.1021/ic500772f | *Inorg. Chem.* 2014, 53, 10835−10845

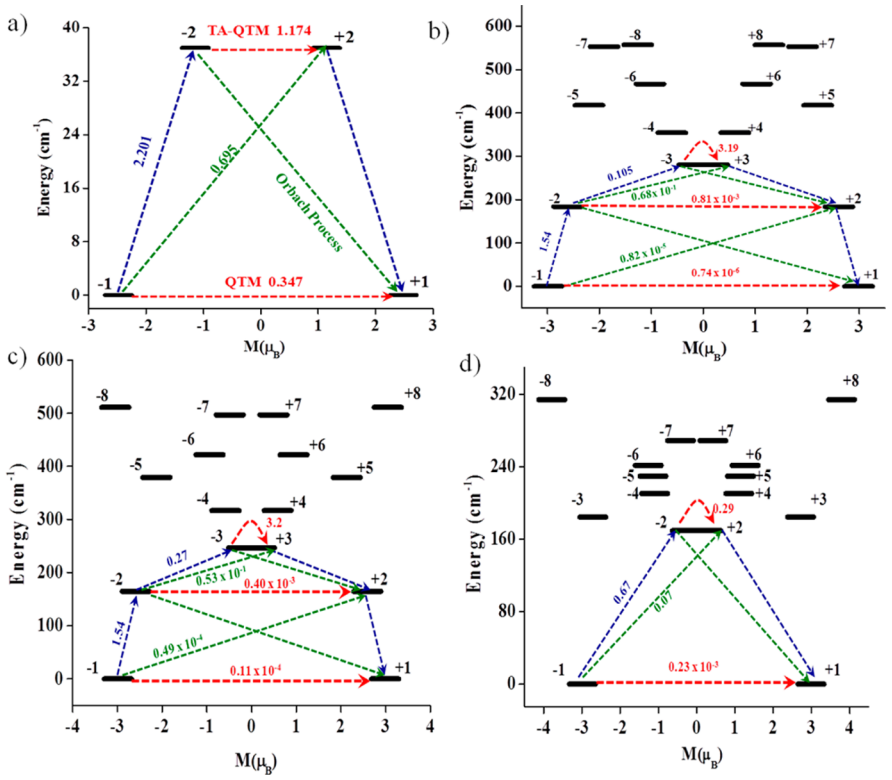

Figure 3. *Ab initio* computed magnetization blocking barrier for all complexes **1**–**4**: (a) complex **1**, (b) complex **2**, (c) complex **3**, and (d) complex **4**. The thick black line indicates the Kramers doublets (KDs), as a function of magnetic moment. The dotted green lines show the possible pathway of the Orbach process. The dotted blue lines show the most probable relaxation pathways for magnetization reversal. The dotted red lines represent the presence of QTM/TA-QTM between the connecting pairs. The numbers provided at each arrow are the mean absolute value for the corresponding matrix element of transition magnetic moment.[42]

mean absolute value of the matrix elements of the transition magnetic moments between the corresponding states. For **1**, the computed g-tensors show significant transverse component with (g_{xx} = 0.6742 , g_{yy} = 1.4119) in the ground state. This clearly suggest that the major relaxation is likely to the be QTM in the ground state. Our calculations also affirm this point as shown in Figure 3a. The next excited KD is located at 37 cm^{-1} and possesses much larger transverse anisotropy. The g_{zz}-axis in this case is found to lie at the intersection of N and O donor ligand and deviates from the ground-state KD by 20°. This activates the Orbach/Raman relaxation via the first excited state and as expected a significant magnetic moment matrix element has also been observed for this process (see Figure 3a).[39] Since the transverse anisotropy of the first excited KD is large, this also leads to a significant TA-QTM process, and this is also reflected in the computed numbers.

The first excited KD in this complex is located at 37 cm^{-1} (53.24 K) higher from the ground state. Since the major relaxation occurs via the first excited state, this gap of 37 cm^{-1} between the ground state and the first excited state can be taken as the U_{eff} value, which can be further directly compared to the reported experimental U_{eff} values.[19] Complex **1** exhibits two relaxations in the AC susceptibility studies, where the first one characterized to be a fast relaxation yields a barrier height of 15.58 K, while the other is a slow relaxation with an effective barrier height of 22.37 K.[19] These two relaxations were attributed to the presence of different conformation of the methyl groups present in the −thd ligands or the presence of two distinct but closely related crystallographic phases. To test this hypothesis of conformational-dependent relaxation, we have modeled a complex from the X-ray structure of **1** (model **1a**) where these methyl groups are kept in eclipsed conformations (see Figures S2 and S6 and Table S4 in the Supporting Information for details). Our calculations on model **1a** also yield exactly the same barrier heights, anisotropies, and energy spectra, compared to the parent complex, and no noticeable electronic differences are witnessed, which supports the conclusion that methyl rotation has no influence on the magnitude of U_{eff} values. This illustrates that the methyl group conformations are not strong enough to perturb the magnetic anisotropy at the Er(III) center. Since methyl groups are not directly attached to the Er(III) center, this is rather expected. However, there are literature precedents where the orientations of the H atoms present at the coordinating water molecules are found to drastically influence the orientation of the *g*-tensors and the magnetic relaxation.[9e] Thus, our rationale here is that the observed slow relaxation could be due to TA-QTM/Orbach/Raman process and thus can be compared to our estimated U_{eff} value of 53.24 K and the fast relaxation is likely to be due to QTM. Other analysis such as conformational/structural optimization with DFT also does not provide a rationale for two relaxation phenomena observed[23] (see Tables S5 and S6, and Figure S3, in the Supporting Information for details).

For complex **2**, the g_{zz}-axis is found to orient along the principal C_8-axis, passing through the center of the COT ligand (see Figure 1b), despite significant negative charges on the carbon atoms (DFT calculations; see Table S7 in the Supporting Information for details). Although the C_2-axes being perpendicular to the C_8 are likely to be in the less

dx.doi.org/10.1021/ic500772f | *Inorg. Chem.* 2014, 53, 10835−10845

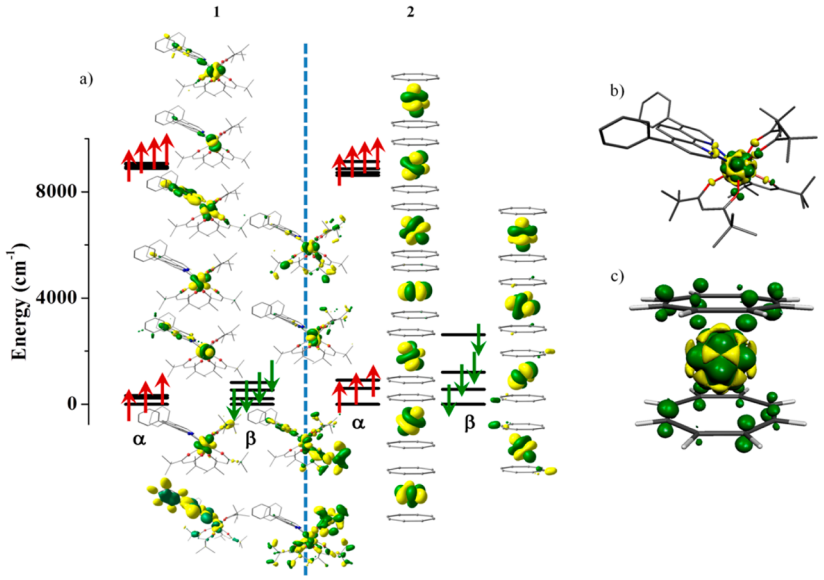

Figure 4. (a) DFT computed α and β MOs representing the 4f-orbitals with their corresponding Eigen values for complexes **1** (left) and **2** (right). DFT computed spin density plot for (b) **1** and (c) **2**. The isodensity surface represented corresponds to a value of 0.005 e^-/bohr^3. The green and yellow regions indicate the positive and negative spin densities, respectively.

repulsive direction, this would not preserve the overall symmetry of the molecule and is not a unique axis of direction for the anisotropy. This is also in accordance with previous observations on similar higher symmetry structures, where the anisotropy is found to align always along the principal axis of symmetry, independent of the electrostatic repulsion.[6] Similar situation is encountered also in complexes **3** and **4** (see Figures 3b and 3c). The energy spectra of the eight low-lying KDs in **2** and **3** are found to spread over a range of 500 cm^{-1}, which is larger than that of complex **4** (ca. 325 cm^{-1}). For complexes **2**−**4**, the computed *g*-tensors are of Ising type (see Table 1 and Tables S8−S13, and Figure S4, in the Supporting Information) with the g_{xx} and g_{yy} values being essentially zero, whereas the g_{zz} values exceed 17.92 in all of the cases. This reveals interesting differences between complex **1** and complexes **2**−**4**, where the later set is found to be superior over complex **1**. The computed U_{eff} values for complexes **2**−**4** are 403.5, 355.5, and 243.5 K, respectively, and this is in agreement with the experimental data (216, 187, and 197 K for **2**, **3**, and **4**, respectively),[22,17c,f] although the computed values are overestimating the U_{eff} values. Discrepancy between computed and the experimental values are expected as the computed values assume inherently no QTM between the ground-state KDs and no intermolecular interactions—these are conditions that are very stringent and difficult to meet. Our calculated U_{eff} values are in good agreement with the earlier reports.[23] We would like to note here that, although no magnetic field has been applied, anisotropy field contribution to the effective magnetic field causes the magnetic moment to be oriented along certain crystallographic directions.[40]

The computed QTM effect between the ground-state KDs in all cases are found to be very small (see Figures 3b−d) with the calculated matrix coefficients increasing in the following order: **2** < **3** < **4**. Interestingly, the computed U_{eff} value has also been found to decrease in the same order. For complexes **2** and **3**, the anisotropy axis of the ground-state KD is found to be collinear with the first five excited KDs. (Note that the deviations are found to be <2°;[6] also see Tables S9 and S11 in the Supporting Information for details). This suggests that the relaxation, in principle, should happen via the sixth KD; however, the $m_J = \pm 1/2$ energy level is found to be stabilized as the second excited state in both cases. This enforces relaxation at this point via TA-QTM process as this possesses a significant transverse anisotropy (see Figures 4b and 4c). Thus, the presence of high symmetry leads to collinear magnetization axis and suppress the magnetization relaxation via the first excited level for complexes **2** and **3**, although the absolute U_{eff} value that is computed varies from experimental observations.[7,16b,14e] On the other hand, in case of complexes **1** and **4**, the noncoincidence of the principal axes of magnetization of ground-state and first excited KDs activates the magnetic relaxation via first excited state KD (see Tables S2 and S13 in the Supporting Information for details). This observed difference in complex **4** is likely to be attributed to the lack of a higher-order symmetry axis and to the fact that the structure is rather bent, with an acute COT−Er−Cp* angle (~170°). The presence of Cp* ligand in **4** causes larger repulsion on the axial direction, and this results in stabilization of low-magnitude m_J orientations as the first excited state. Besides, the first excited state is tilted, with respect to the ground state, and this activates relaxation to be operative via the first excited state.

To gain more insight into the mechanism of magnetic relaxation, we have also computed the crystal field parameters. Assuming that intermolecular and hyperfine interactions are small or negligible, the probability of QTM between the ground-state KDs is best described by the crystal field (CF) parameters.[5b,41,50,51] The corresponding crystal field Hamiltonian is given as $H_{CF} = B_k^q O_k^q$, where B_k^q is the crystal field parameter while O_k^q is the Steven's operator. The QTM effects are expected to be dominant in a system where the nonaxial B_k^q (where $k \neq 0$, and $q = 2, 4, 6$) terms are larger than the axial B_k^q (where $k = 0$, and $q = 2, 4, 6$) terms. The computed CF parameters for all four complexes **1**−**4** are given in Table S14 in the Supporting Information. In the case of complex **1**, a significant transverse anisotropy has been observed (g_{xx} = 0.6742, g_{yy} = 1.4119) for the ground state and this is reflected in computed CF parameters, where the nonaxial B_2^1, B_2^2, B_4^{-3}, and

dx.doi.org/10.1021/ic500772f | Inorg. Chem. 2014, 53, 10835−10845

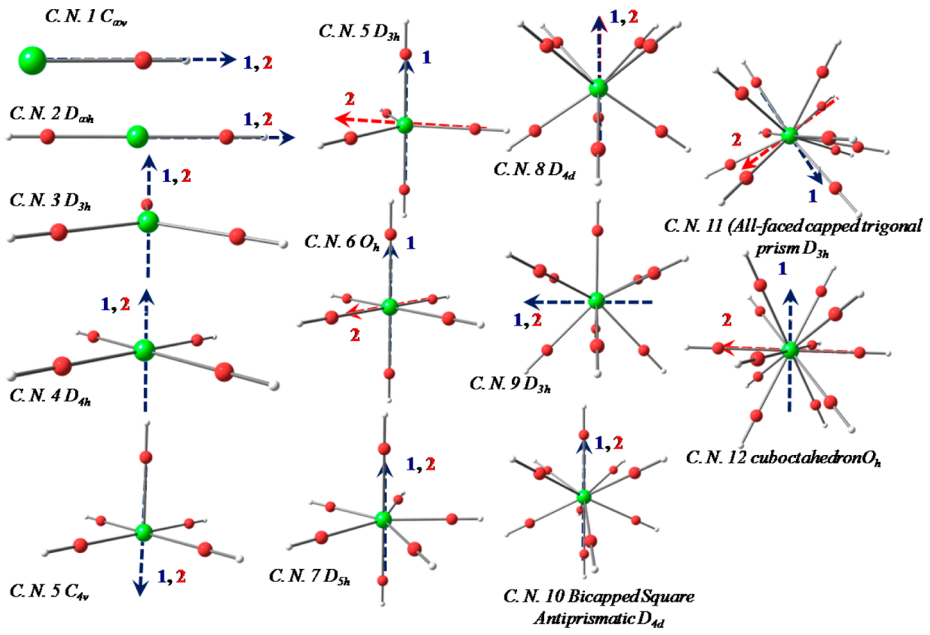

Figure 5. *Ab initio* computed principal magnetization axes of all the model complexes from C.N.1 to C.N.2. Dashed blue lines shown in the figures are calculated main magnetic of the ground-state Kramer doublet (**1**), while dashed red lines are main magnetic of the first excited state Kramer doublet (**2**).

B_6^5 terms are significantly larger than the axial terms (B_2^0, B_4^0, B_6^0; see Table S14 in the Supporting Information). The lack of crystallographic symmetry and asymmetric CF interactions leads to large transverse anisotropy, and this activates the ground-state QTM effect, which destroys the SMM behavior. The application of the magnetic field lifts the degeneracy of the $\pm m_J$ levels leading to the suppression of QTM effect and observation of field-induced SMM characteristics with two relaxation phenomena. Although the applied magnetic field reduces the ground-state QTM effects to a certain extent, other relaxation processes are still dominant, leading to a very small U_{eff} value for complex **1**. On the other hand, the computed CF parameters for complexes **2** and **3** reveal that axial terms are relatively large for this set of complexes. Quite interestingly, the axial $B_{2,4,6}^0$ terms are found to decrease in the same order (**2** > **3** > **4** > **1**) as that of the computed U_{eff} value.

This is clearly correlated to the point group symmetry of complexes **1**−**4**. Particularly, the axial terms are found to be more than an order of magnitude larger, compared to the nonaxial terms for complexes **2** and **3**, while complexes **1** and **4** possess significant nonaxial terms. It is noteworthy to mention here that the B_k^q parameters are vanishing in the presence of high symmetry, and this opens up a viable way to control the QTM by fine-tuning the local symmetry around the metal ions.

To further understand the role of CF parameters and the 4f-ligand interactions, we have analyzed the 4f orbital energies, charges, and spin densities obtained from DFT calculations. Attention has been paid particularly to complexes **1** and **2**. In **2**, all the carbon atoms are found to carry equal negative charge of −0.12, whereas in **1**, a positive charge exists on nitrogen atoms and a significant negative charge is present on oxygen atoms (see Tables S3 and S7 in the Supporting Information for details). The computed spin density plots for **1** and **2** are shown in Figures 4b and 4c. Interestingly, for complex **1**, a mixture of spin delocalization and polarization is detected with predominant spin polarization on the nitrogen donor atoms. For complex **2**, a dominant spin delocalization with significant spin densities on the π-orbitals of the COT ligands has been observed. Thus, the way the spins are propagated within these two molecules are markedly different. This is in fact attributed to the difference in bonding between **1** and **2**. The computed MO diagram for the 4f orbitals along with their energies for **1** and **2** are shown in Figure 4a. In both complexes, the 4f α-orbitals are found to split, but the interaction with the ligands is particularly visible in complex **1**. Of particular interest are the four β-orbitals energies where larger splitting is detected with complex **2** than complex **1**. Since the 4f β-orbital densities are correlated to the ground-state m_J levels,[36b] this splitting is further analyzed. In complex **2**, the COT σ*-orbitals are found to interact with the 4f β-orbitals and the orbital ordering are found to relate to the nature of the interaction with the σ*-orbitals and the number of nodal planes present in them. For complex **1**, however, the interactions are not very strong and this might be related to the orbital energies and the ligand donor abilities.

Apart from the SMM behavior, lanthanide complexes also exhibit luminescence properties.[2e,9a,12b] This is particularly true for the Er(III) complexes, which exhibit characteristic features, and these transitions reveal intrinsic details of magnetic anisotropy,[9e] as well as lanthanide−ligand bonding interactions. Characteristic luminescence spectrum for complex **1** in diluted methanol solution has been reported.[19] Two peaks of significance are observed: one at 289 nm and another at 342 nm.[19] Furthermore, several f-f transitions have also been observed in the range of 400−700 nm. To gain insights into these two particular intense transitions, we have performed time-dependent DFT (TD-DFT) calculations on the organic ligand backbone using ORCA suite of program, although this method is very qualitative, the computed transitions are found to be in agreement with the experimental results (for more details, see the Supporting Information and, in particular, Figure S5).

Role of Geometry and the Coordination Numbers on the U_{eff} Values: Building Highly Anisotropic SMMs. Since

dx.doi.org/10.1021/ic500772f | *Inorg. Chem.* 2014, 53, 10835−10845

the effect of ligand field and the role of symmetry[5b,14b] on the magnetic relaxation on Er(III)-based SIMs are already established, here, we have taken one step forward to predict the role of point group symmetry and the coordination number on the computed magnetic anisotropy. To best of our knowledge, there are no such quantitative studies reported in the literature, where *in silico* fine tunings are attempted. There are certainly two factors at play for the fine tuning of the magnetic anisotropy. The first, being the electrostatic potential of the ligands and its importance, has been discussed at length for Dy(III) SMMs earlier.[7b,15c,36] In this context, the ligand field approach popularized by Long et al.[3e] must be mentioned, since this is frequently used to rationalize the presence/absence of SMM characteristics in lanthanide-based molecular magnets. However, this approach inherently assumes the absence of QTM/TA-QTM effects, which are found to be the major relaxation mechanism for the lanthanide-based molecular magnets.[43] The second factor at play here is the coordination symmetry, where highly symmetric lanthanide complexes are found to be superior in exhibiting SMM characteristics. Although the importance of this factor in dictating SMM characteristics has been realized earlier, the potential of this effect on the magnetic relaxation has not been explored in detail.[3e,6,17f] Interestingly, complex **2** shows the second-largest T_B value for any SMM; however, the ligand field effects of the COT ligands are ideally suited to enhance the SMM character of oblate ions.[17f] This suggests that perhaps controlling symmetry in a given complex is more important than fine-tuning the electrostatic potential of the ligands. This is clearly manifested in the magnetic properties of complexes **3** and **4**, where the symmetry loss leads to a significant reduction in the observed U_{eff} values. Keeping this in mind, we have decided to explore the role of coordination numbers on the magnetic anisotropy, and this has been done by modeling structures with varying coordination numbers, from 1 to 12. All of the model structures are generated also by maintaining the closest higher-order symmetry to achieve large U_{eff} values. For this purpose, we have chosen $[Er(OH)_n]^{m\mp}$ models where the Er−O distances are kept at 2.3 Å, the O−H bond distances are fixed at 1 Å, and the Er−O−H bond angle(s) are fixed at 180° to preserve the symmetry for all of the models. We would like to note here that the models considered here are fictitious and are employed here only to probe the role of symmetry and coordination number; however, the linear coordination tested here might be achievable with ligands such as cyanides.[44] Models studied here are shown in Figure 5, along with the computed g_{zz} anisotropy axis and the energies of low-lying eight KDs for model complexes from C.N.1 to C.N.12 are provided in the Supporting Information (see Table S16).

The following points emerge from our predictions:

(i) The C.N.1 and C.N.2 ($C_{\infty v}$ and $D_{\infty h}$) models do not possess any equatorial ligation, because of which the $m_J = \pm 1/2$ level becomes the ground state. This state has large transverse anisotropy and therefore is unlikely to yield any SMM character. This is contrary to what has been proposed for the Dy(III) SMMs,[14c] and this is also well-reproduced in our computational studies on Dy(III) model analogues (see the Supporting Information for details).

(ii) High symmetry such as D_{3h} and D_{4h} associated with C.N.3 and C.N.4 offer a large magnetic anisotropy and possess an Ising-type ground state with the g_{zz} passing always through the principal axis of symmetry. Because of the high symmetry, the colinearity of the g_{zz} axis is maintained for all the eight KDs, leading to a large U_{eff} value measured as the gap between the ground state and the highest excited state. However, as the electrostatic potential on the $-xy$ plane increases with increasing coordination number, the U_{eff} value for the C.N.4 model has been found to be higher, compared to the C.N.3 model (see the Table S16 in the Supporting Information for details). Thus, our calculations predict a barrier height of nearly 1150 K for the four coordinate models with D_{4h} symmetry (see Figure 5). Although low-coordination-number lanthanide complexes are reported as early as in the 1990s,[45] the magnetic properties have not been thoroughly measured. A recent report by Tang et al. sheds light on this issue where the three-coordinated Er(III) complex is found to be a superior SMM with U_{eff} = 120 K.[46] This strongly supports our predictions.

(iii) The addition of more ligands is assumed to occur in the axial direction for C.N.5−C.N.7. Since addition along the axial direction is unfavorable for the prolate ions, this alters the m_J levels. For C.N.5, square pyramidal geometry and trigonal bipyramidal geometries are modeled where square pyramidal structure is found to yield larger U_{eff}, compared to trigonal bipyramidal D_{3h} structure. In the D_{3h} structure, the two axial ligands destabilize the $m_J = \pm 15/2$ states and lower m_J levels become the ground state which bring forth a large transverse anisotropy. A similar situation is encountered also for the C.N.6 and C.N.7 models (see Table S16 in the Supporting Information), although for the C.N.7 model, large m_J is getting stabilized, which leads to the expectation of moderate SMM behavior for this structure. This is similar to the case reported for Dy(III) complexes where D_{5h} point group molecules are predicted to be superior to the O_h point group structure.[5b]

(iv) For C.N.8, a square antiprismatic structure with the D_{4d} point group is assumed. Since all the ligands are nonaxial, the prolate density faces repulsion only on the edges and this certainly improves the magnetic behavior with $m_J = \pm 15/2$ and $m_J = \pm 13/2$ as the ground state and the first excited state, respectively. However, the repulsion on the edges stabilizes $m_J = \pm 1/2$ as the second excited state and this enforces relaxation via this state and brings down the net U_{eff} values. This essentially yields an "M" shape energy level and a similar energy pattern has been observed also for complex **2**.

(v) Higher coordination number (i.e., >8) does not offer significant improvement because the additional ligands occupy the axial positions.

(vi) A similar model study has also been undertaken for Dy(III) ion (see Figure S7 and Table S16 in the Supporting Information) for comparison. Among all the models studied for the Dy(III), the C.N.2 model ($D_{\infty h}$ symmetry) is found to have the largest effective barrier height (U_{eff} = 3035 K). This is due to the collinearity of all the excited KDs, with respect to the ground-state KDs. Remarkably, the CN 2 model of Er(III) does not expect to exhibit any SMM behavior, because of the absence of equatorial ligation, whereas the same model with Dy(III) shows the largest effective barrier for magnetization reversal. This difference observed is attributed to the nature of f-electron density in both ions, i.e., prolate vs oblate for Dy(III) and Er(III) ions, respectively. (The energy barrier for magnetization reversal in the $[Er(OH)_4]^-$ model complex is shown in Figure 6; for a discussion of other Dy(III) models, see the Supporting Information).

Overall, the model studies suggest that maintaining symmetry is extremely important, because this yields a complete collinearity of the principal magnetization axes among all the KDs. This enhances the U_{eff} value significantly.

dx.doi.org/10.1021/ic500772f | Inorg. Chem. 2014, 53, 10835−10845

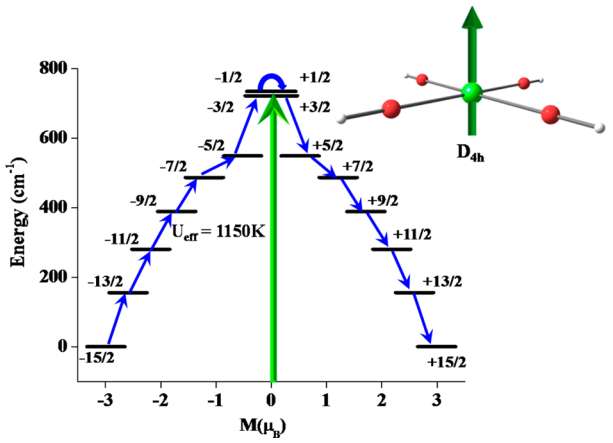

Figure 6. Energy barrier for magnetization reversal in $[Er(OH)_4]^-$ model complex. The thick black line indicates the Kramers doublet (KDs) as a function of the magnetic moment. The blue arrows show the path for reorientation of magnetization.

However, higher symmetry does not always translate to higher U_{eff} values if the ligands occupy an axial direction. Thus, achieving control over both the structure and symmetry is important for future success.

4. CONCLUSIONS

Among the lanthanides, Er(III) complexes have been gaining attention in recent years, because several of the single-molecule magnets (SMMs) that have been reported are Er(III)-based and they possess a larger barrier height for magnetization reversal. Here, we have performed extensive *ab initio* calculations on four Er(III) complexes in order to shed light on the magnetic properties and the magnetic relaxation. The conclusions derived from this work are summarized below.

(1) Among the four complexes chosen, complex **1** is a eight-coordinated heterolyptic-O/N ligand-based Er(III) complex that possesses a significant transverse anisotropy at the ground state and the first excited state. This activates the QTM mechanism for magnetic relaxation, and, thus, this complex exhibits SMM behavior only in the presence of an applied field. The reason for this behavior was attributed to a lack of higher-order symmetry and coordination environment. Two relaxations observed experimentally in this complex are assigned to the QTM and Orbach/TA-QTM/Raman processes.

(2) The high symmetry present in complex **2** leads to pure Ising anisotropy for the ground state and the g_{zz} axis of the ground state and the first excited states are found to be collinear. This collinearity between the states leads to suppression of relaxation via the first excited m_J level and magnetization relaxation is found to occur from the second excited $m_J = \pm 1/2$ state. This leads to relatively larger U_{eff} and T_B values for this complex. The bonding aspects and the computed spin densities reveal that **1** and **2** are intrinsically different both in the nature of the Er−ligand interaction and in the shape of the Stark energy levels.

(3) Although a similar mechanism is operational for **3**, this complex possesses lower symmetry, compared to **2**. This reduces the ground-state−excited-state gap and, hence, the U_{eff} values. Larger structural distortion and the bent nature of the COT−Er−Cp* angle in complex **4** enhances the asymmetric environment, leading to stabilization of the $m_J = \pm 1/2$ orientation as the first excited state. This results in the further reduction in the U_{eff} values, compared to complexes **2** and **3**.

(4) Our detailed studies on model complexes of Er(III) by varying the coordination number from 1 to 12 reveal that the presence of ligand interaction on the equatorial plane and high symmetry are the two favorable conditions to obtain large U_{eff} values. The absence of axial ligands is much more crucial than symmetry conditions, because this activates the QTM effect by stabilizing lower m_J levels as the ground state or close-lying excited state. Among all the tested models, a three-coordinated D_{3h} model and a four-coordinated D_{4h} model are found to possess the largest barrier height, which is followed by a moderate barrier height for models such as C_{4v} (C.N.5), D_{5h} (C.N.7), and D_{4d} (C.N.8) and lowest barrier height observed for models such as D_{3h} (C.N.11), D_{4d} (C.N.10), D_{3h} (C.N.9), D_{3h} (C.N.5), O_h (C.N.6), O_h (C.N.12), $D_{\infty h}$ (C.N.2) and $C_{\infty v}$ (C.N.1) (in the order of decreasing U_{eff} values) . We believe that these calculations might be a useful synthetic target for experimentalists in the design of novel Er(III)-based SIMs.

■ ASSOCIATED CONTENT

Ⓢ Supporting Information

CASSCF+RASSI computed spin-free and spin−orbit energies for complexes **1**−**4** (Tables S1, S8, S10, and S12, and Figure S4); energies of all of the low-lying KDs, along with the computed *g*-anisotropies for complexes **1**−**4** (Tables S2, S4, S6, S9, S11, and S13); orientation of the computed KDs for complex **1** (Figure S1); DFT-computed NPA spin density values, *xyz* coordinates for the DFT optimized structures (Tables S3 and S5, and Figure S3); computed crystal field parameters for complex **1** (Table S14); TD-DFT computed absorptions along with oscillator strength and simulated spectra and relevant brief discussion (Table S15 and Figure S5); low-lying KDs energies for different Er(III) and Dy(III) models studied (Tables S16 and S17); orientation of the computed KD for the Dy(III) models (Figures S7−S9); and ground-state and first-excited-state orientation for complexes **1**−**4** (Figure S10). This material is available free of charge via the Internet at http://pubs.acs.org.

■ AUTHOR INFORMATION

Corresponding Author

*Tel.: +91-22-2576 7183. Fax: +91-22-2576 7152. E-mail: rajaraman@chem.iitb.ac.in.

Notes

The authors declare no competing financial interest.

■ ACKNOWLEDGMENTS

G.R. acknowledges financial support from DST, India (Nos. SR/S1/IC-41/2010 and SR/NM/NS-1119/2011) and IITB for High Performance Computing Facility. S.K.S. and T.G. thank CSIR and UGC New Delhi for a SRF fellowship. We would like to thank Prof. L. F. Chibotaru (Theory of Nanomaterials Group, Department of Chemistry, Katholieke Universiteit Leuven, Belgium) for his MOLCAS routine, which enabled us to calculate the transition matrix elements.

■ REFERENCES

(1) Ishikawa, N.; Sugita, M.; Ishikawa, T.; Koshihara, S.; Kaizu, Y. *J. Am. Chem. Soc.* **2003**, *125*, 8694−8695.

(2) (a) Takamatsu, S.; Ishikawa, T.; Koshihara, S. Y.; Ishikawa, N. *Inorg. Chem.* **2007**, *46*, 7250−7252. (b) Gatteschi, D.; SessoliR.; Villain, J. In *Molecular Nanomagnets*; Oxford University Press: Oxford,

U.K., 2006. (c) Christou, G.; Gatteschi, D.; Hendrickson, D. N.; Sessoli, R. *MRS Bull.* **2000**, *25*, 66−71. (d) Sessoli, R.; Gatteschi, D.; Caneschi, A.; Novak, M. A. *Nature* **1993**, *365*, 141−143. (e) Luzon, J.; Sessoli, R. *Dalton Trans.* **2012**, *41*, 13556−13567. (f) Sorace, L.; Benelli, C.; Gatteschi, D. *Chem. Soc. Rev.* **2011**, *40*, 3092−3104. (g) Guo, Y. N.; Xu, G. F.; Guo, Y.; Tang, J. K. *Dalton Trans.* **2011**, *40*, 9953−9963. (h) Ishikawa, N. *Polyhedron* **2007**, *26*, 2147−2153.

(3) (a) Woodruff, D. N.; Winpenny, R. E.; Layfield, R. A. *Chem. Rev.* **2013**, *113*, 5110−5148. (b) Woodruff, D. N.; Tuna, F.; Bodensteiner, M.; Winpenny, R. E. P.; Layfield, R. A. *Organometallics* **2013**, *32*, 1224−1229. (c) Zhang, P.; Zhang, L.; Xue, S.; Lin, S.; Tang, J. *Chin. Sci. Bull.* **2012**, *57*, 2517−2524. (d) Mondal, K. C.; Sundt, A.; Lan, Y.; Kostakis, G. E.; Waldmann, O.; Ungur, L.; Chibotaru, L. F.; Anson, C. E.; Powell, A. K. *Angew. Chem., Int. Ed. Engl.* **2012**, *51*, 7550−7554. (e) Rinehart, J. D.; Long, J. R. *Chem. Sci.* **2011**, *2*, 2078−2085. (f) Sessoli, R.; Powell, A. K. *Coord. Chem. Rev.* **2009**, *253*, 2328−2341.

(4) (a) Aromi, G.; Aguila, D.; Gamez, P.; Luis, F.; Roubeau, O. *Chem. Soc. Rev.* **2012**, *41*, 537−546. (b) Winpenny, R. E. P. *Angew. Chem., Int. Ed.* **2008**, *47*, 7992−7994. (c) Ardavan, A.; Rival, O.; Morton, J. J. L.; Blundell, S. J.; Tyryshkin, A. M.; Timco, G. A.; Winpenny, R. E. P. *Phys. Rev. Lett.* **2007**, *98*, 057201−057204. (d) Affronte, M.; Troiani, F.; Ghirri, A.; Candini, A.; Evangelisti, M.; Corradini, V.; Carretta, S.; Santini, P.; Amoretti, G.; Tuna, F.; Timco, G.; Winpenny, R. E. P. *J. Phys. D: Appl. Phys.* **2007**, *40*, 2999−3004. (e) Leuenberger, M. N.; Loss, D. *Physica E* **2001**, *10*, 452−457. (f) Coronado, E.; Day, P. *Chem. Rev.* **2004**, *104*, 5419. (g) Bogani, L.; Wernsdorfer, W. *Nat. Mater.* **2008**, *7*, 179−186. (h) Baldoví, J. J.; Cardona-Serra, S.; Clemente-Juan, J. M.; Coronado, E.; Gaita-Ariño, A.; Palii, A. *Inorg. Chem.* **2012**, *51*, 12565−12574.

(5) (a) Wang, Z.-G.; Lu, J.; Gao, C.-Y.; Wang, C.; Tian, J.-L.; Gu, W.; Liu, X.; Yan, S.-P. *Inorg. Chem. Commun.* **2013**, *27*, 127−130. (b) Liu, J.-L.; Chen, Y.-C.; Zheng, Y.-Z.; Lin, W.-Q.; Ungur, L.; Wernsdorfer, W.; Chibotaru, L. F.; Tong, M.-L. *Chem. Sci.* **2013**, *4*, 3310−3316. (c) Chen, G. J.; Guo, Y. N.; Tian, J. L.; Tang, J.; Gu, W.; Liu, X.; Yan, S. P.; Cheng, P.; Liao, D. Z. *Chem.—Eur. J.* **2012**, *18*, 2484−2487. (d) Cardona-Serra, S.; Clemente-Juan, J. M.; Coronado, E.; Gaita-Arino, A.; Camon, A.; Evangelisti, M.; Luis, F.; Martinez-Perez, M. J.; Sese, J. *J. Am. Chem. Soc.* **2012**, *134*, 14982−14990.

(6) Blagg, R. J.; Ungur, L.; Tuna, F.; Speak, J.; Comar, P.; Collison, D.; Wernsdorfer, W.; McInnes, E. J. L.; Chibotaru, L. F.; Winpenny, R. E. P. *Nat. Chem.* **2013**, *5*, 673−678.

(7) (a) Xiong, G.; Qin, X.-Y.; Shi, P.-F.; Hou, Y.-L.; Cui, J.-Z.; Zhao, B. *Chem. Commun.* **2014**, *50*, 4255−4257 (DOI: 10.1039/c3cc49342c). (b) Langley, S. K.; Wielechowski, D. P.; Vieru, V.; Chilton, N. F.; Moubaraki, B.; Abrahams, B. F.; Chibotaru, L. F.; Murray, K. S. *Angew. Chem., Int. Ed. Engl.* **2013**, *52*, 12014−12019. (c) Colacio, E.; Ruiz, J.; Mota, A. J.; Palacios, M. A.; Ruiz, E.; Cremades, E.; Hänninen, M. M.; Sillanpää, R.; Brechin, E. K. *C. R. Chim.* **2012**, *15*, 878−888. (d) Baskar, V.; Gopal, K.; Helliwell, M.; Tuna, F.; Wernsdorfer, W.; Winpenny, R. E. *Dalton Trans.* **2010**, *39*, 4747−4750. (e) Zhang, C.; Chen, Y.; Ma, H.; Yu, T.; Liu, B.; Pang, H. *New J. Chem.* **2013**, *37*, 1364−1370. (f) Murugesu, M.; Mishra, A.; Wernsdorfer, W.; Abboud, K. A.; Christou, G. *Polyhedron* **2006**, *25*, 613−625. (g) Mishra, A.; Wernsdorfer, W.; Parsons, S.; Christou, G.; Brechin, E. K. *Chem. Commun. (Cambridge)* **2005**, 2086−2088. (h) Osa, S.; Kido, T.; Matsumoto, N.; Re, N.; Pochaba, A.; Mrozinski, J. *J. Am. Chem. Soc.* **2004**, *126*, 420−421.

(8) (a) Murakami, R.; Nakamura, T.; Ishida, T. *Dalton Trans* **2014**, *43*, 5893−5898. (b) Mei, X. L.; Wang, X. F.; Wang, J. J.; Ma, Y.; Li, L. C.; Liao, D. Z. *New J. Chem.* **2013**, *37*, 3620−3626. (c) Gao, Y.-y.; Wang, Y.-l.; Hu, P.; Yang, M.-f.; Ma, Y.; Wang, Q.-l.; Li, L.-c.; Liao, D.-z. *Inorg. Chem. Commun.* **2013**, *27*, 31−35. (d) Rinehart, J. D.; Fang, M.; Evans, W. J.; Long, J. R. *Nat. Chem.* **2011**, *3*, 538−542. (e) Rinehart, J. D.; Fang, M.; Evans, W. J.; Long, J. R. *J. Am. Chem. Soc.* **2011**, *133*, 14236−14239. (f) Wang, X. L.; Li, L. C.; Liao, D. Z. *Inorg. Chem.* **2010**, *49*, 4735−4737. (g) Xu, J.-X.; Ma, Y.; Liao, D.-z.; Xu, G.-F.; Tang, J.; Wang, C.; Zhou, N.; Yan, S.-P.; Cheng, P.; Li, L.-C. *Inorg. Chem.* **2009**, *48*, 8890−8896. (h) Mei, X.-L.; Ma, Y.; Li, L.-C.; Liao, D.-Z. *Dalton Trans.* **2012**, *41*, 505−511.

(9) (a) Wang, Y.-L.; Ma, Y.; Yang, X.; Tang, J.; Cheng, P.; Wang, Q.-L.; Li, L.-C.; Liao, D.-Z. *Inorg. Chem.* **2013**, *52*, 7380−7386. (b) Ren, M.; Pinkowicz, D.; Yoon, M.; Kim, K.; Zheng, L. M.; Breedlove, B. K.; Yamashita, M. *Inorg. Chem.* **2013**, *52*, 8342−8348. (c) Menelaou, M.; Ouharrou, F.; Rodriguez, L.; Roubeau, O.; Teat, S. J.; Aliaga-Alcalde, N. *Chem.—Eur. J.* **2012**, *18*, 11545−11549. (d) Guo, P. H.; Liu, J. L.; Zhang, Z. M.; Ungur, L.; Chibotaru, L. F.; Leng, J. D.; Guo, F. S.; Tong, M. L. *Inorg. Chem.* **2012**, *51*, 1233−1235. (e) Cucinotta, G.; Perfetti, M.; Luzon, J.; Etienne, M.; Car, P. E.; Caneschi, A.; Calvez, G.; Bernot, K.; Sessoli, R. *Angew. Chem., Int. Ed. Engl.* **2012**, *51*, 1606−1610. (f) Habib, F.; Lin, P. H.; Long, J.; Korobkov, I.; Wernsdorfer, W.; Murugesu, M. *J. Am. Chem. Soc.* **2011**, *133*, 8830−8833. (g) Guo, Y. N.; Xu, G. F.; Wernsdorfer, W.; Ungur, L.; Guo, Y.; Tang, J. K.; Zhang, H. J.; Chibotaru, L. F.; Powell, A. K. *J. Am. Chem. Soc.* **2011**, *133*, 11948−11951. (h) Blagg, R. J.; Muryn, C. A.; McInnes, E. J. L.; Tuna, F.; Winpenny, R. E. P. *Angew. Chem., Int. Ed.* **2011**, *50*, 6530−6533. (i) Li, D. P.; Wang, T. W.; Li, C. H.; Liu, D. S.; Li, Y. Z.; You, X. Z. *Chem. Commun.* **2010**, *46*, 2929−2931. (j) Ke, H.; Xu, G. F.; Guo, Y. N.; Gamez, P.; Beavers, C. M.; Teat, S. J.; Tang, J. *Chem. Commun.* **2010**, *46*, 6057−6059. (k) Jiang, S. D.; Wang, B. W.; Su, G.; Wang, Z. M.; Gao, S. *Angew. Chem., Int. Ed.* **2010**, *49*, 7448−7451. (l) Hewitt, I. J.; Tang, J.; Madhu, N. T.; Anson, C. E.; Lan, Y.; Luzon, J.; Etienne, M.; Sessoli, R.; Powell, A. K. *Angew. Chem., Int. Ed.* **2010**, *49*, 6352−6356. (m) Bernot, K.; Luzon, J.; Bogani, L.; Etienne, M.; Sangregorio, C.; Shanmugam, M.; Caneschi, A.; Sessoli, R.; Gatteschi, D. *J. Am. Chem. Soc.* **2009**, *131*, 5573−5579. (n) Lin, P. H.; Burchell, T. J.; Clerac, R.; Murugesu, M. *Angew. Chem., Int. Ed.* **2008**, *47*, 8848−8851. (o) Lin, P. H.; Burchell, T. J.; Ungur, L.; Chibotaru, L. F.; Wernsdorfer, W.; Murugesu, M. *Angew. Chem., Int. Ed.* **2009**, *48*, 9489−9492.

(10) Chibotaru, L. F.; Ungur, L.; Soncini, A. *Angew. Chem., Int. Ed. Engl.* **2008**, *47*, 4126−4129.

(11) Note: These are quadrupole moment of the f-electron charge cloud, where prolate electron density signifies that the electron charge cloud is axially elongated, the preferred geometry is equatorially coordinated, and, for oblate electron density, the electron charge cloud is equatorially expanded; the crystal field should lie above and below the XY plane.

(12) (a) Wang, Y.-L.; Gu, B.; Ma, Y.; Xing, C.; Wang, Q.-L.; Li, L.-C.; Cheng, P.; Liao, D.-Z. *CrystEngComm* **2014**, *16*, 2283−2289. (b) Pointillart, F.; Le Guennic, B.; Cauchy, T.; Golhen, S.; Cador, O.; Maury, O.; Ouahab, L. *Inorg. Chem.* **2013**, *52*, 5978−5990. (c) Liang, L.; Peng, G.; Li, G.; Lan, Y.; Powell, A. K.; Deng, H. *Dalton Trans.* **2012**, *41*, 5816−5823. (d) Yamase, T. *Chem. Rev.* **1998**, *98*, 307−325.

(13) Note: In lanthanide chemistry, the splitting of the mJ states due to the weak crystal field is often referred to as the Stark splitting, and the states themselves are referred to as Stark sublevels.

(14) (a) Leng, J. D.; Liu, J. L.; Zheng, Y. Z.; Ungur, L.; Chibotaru, L. F.; Guo, F. S.; Tong, M. L. *Chem. Commun.* **2013**, *49*, 158−160. (b) Ungur, L.; Chibotaru, L. F. *Phys. Chem. Chem. Phys.* **2011**, *13*, 20086−20090. (c) Swerts, B.; Chibotaru, L. F.; Lindh, R.; Seijo, L.; Barandiaran, Z.; Clima, S.; Pierloot, K.; Hendrickx, M. F. A. *J. Chem. Theory Comput.* **2008**, *4*, 586−594. (d) Ungur, L.; Van den Heuvel, W.; Chibotaru, L. F. *New J. Chem.* **2009**, *33*, 1224−1229. (e) Ungur, L.; Le Roy, J. J.; Korobkov, I.; Murugesu, M.; Chibotaru, L. F. *Angew. Chem., Int. Ed. Engl.* **2014**, *53*, DOI: 10.1002/anie.201310451. (f) Chibotaru, L.; Ceulemans, A.; Bolvin, H. *Phys. Rev. Lett.* **2008**, *101*, 033003−4.

(15) (a) Leng, J. D.; Liu, J. L.; Lin, W. Q.; Gómez-Coca, S.; Aravena, D.; Ruiz, E.; Tong, M. L. *Chem. Commun.* **2013**, *49*, 9341−9343. (b) Cremades, E.; Ruiz, E. *Inorg. Chem.* **2011**, *50*, 4016−4020. (c) Chilton, N. F.; Langley, S. K.; Moubaraki, B.; Soncini, A.; Batten, S. R.; Murray, K. S. *Chem. Sci.* **2013**, *4*, 1719−1730. (d) Jung, J.; da Cunha, T. T.; Le Guennic, B.; Pointillart, F.; Pereira, C. L. M.; Luzon, J.; Golhen, S.; Cador, O.; Maury, O.; Ouahab, L. *Eur. J. Inorg. Chem.* **2014**, *2014*, 3888−3894 (DOI: 10.1002/ejic.201400121).

(16) (a) Ghosh, S.; Datta, S.; Friend, L.; Cardona-Serra, S.; Gaita-Arino, A.; Coronado, E.; Hill, S. *Dalton Trans.* **2012**, *41*, 13697−

13704. (b) Baniodeh, A.; Lan, Y.; Novitchi, G.; Mereacre, V.; Sukhanov, A.; Ferbinteanu, M.; Voronkova, V.; Anson, C. E.; Powell, A. K. *Dalton Trans.* **2013**, *42*, 8926−8938. (c) Marx, R.; Moro, F.; Dorfel, M.; Ungur, L.; Waters, M.; Jiang, S. D.; Orlita, M.; Taylor, J.; Frey, W.; Chibotaru, L. F.; van Slageren, J. *Chem. Sci.* **2014**, *5*, 3287−3293. (d) Luzon, J.; Bernot, K.; Hewitt, I. J.; Anson, C. E.; Powell, A. K.; Sessoli, R. *Phys. Rev. Lett.* **2008**, *100*, 247204−5. (e) Pedersen, K. S.; Ungur, L.; Sigrist, M.; Sundt, A.; Schau-Magnussen, M.; Vieru, V.; Mutka, H.; Rols, S.; Weihe, H.; Waldmann, O.; Chibotaru, L. F.; Bendix, J.; Dreiser, J. *Chem. Sci.* **2014**, *5*, 1650−1660.

(17) (a) Koo, B. H.; Lim, K. S.; Ryu, D. W.; Lee, W. R.; Koh, E. K.; Hong, C. S. *Chem. Commun.* **2012**, *48*, 2519−2521. (b) Feltham, H. L. C.; Klöwer, F.; Cameron, S. A.; Larsen, D. S.; Lan, Y.; Tropiano, M.; Faulkner, S.; Powell, A. K.; Brooker, S. *Dalton Trans.* **2011**, *40*, 11425−11432. (c) Le Roy, J. J.; Korobkov, I.; Murugesu, M. *Chem. Commun.* **2014**, *50*, 1602−1604. (d) Girginova, P. I.; Pereira, L. C. J.; Coutinho, J. T.; Santos, I. C.; Almeida, M. *Dalton Trans.* **2014**, *43*, 1897−1905. (e) Zhang, Y. Q.; Luo, C. L.; Wang, B. W.; Gao, S. *J. Phys. Chem. A* **2013**, *117*, 10873−10880. (f) Meihaus, K. R.; Long, J. R. *J. Am. Chem. Soc.* **2013**, *135*, 17952−17957. (g) Yamashita, A.; Watanabe, A.; Akine, S.; Nabeshima, T.; Nakano, M.; Yamamura, T.; Kajiwara, T. *Angew. Chem., Int. Ed.* **2011**, *50*, 4016−4020.

(18) Silva, M. R.; Martín-Ramos, P.; Coutinho, J. T.; Pereira, L. C. J.; Martín-Gil, J. *Dalton Trans.* **2014**, *43*, 6752−6761 (DOI: 10.1039/c4dt00168k).

(19) Martín-Ramos, P.; Ramos Silva, M.; Coutinho, J. T.; Pereira, L. C. J.; Chamorro-Posada, P.; Martín-Gil, J. *Eur. J. Inorg. Chem.* **2014**, *2014*, 511−517.

(20) Note: Single-molecule magnets (SMMs) in which prominent slow relaxation of magnetization has been observed upon application of magnetic field, compared to that in zero field.

(21) (a) Ishida, T.; Watanabe, R.; Fujiwara, K.; Okazawa, A.; Kojima, N.; Tanaka, G.; Yoshii, S.; Nojiri, H. *Dalton Trans.* **2012**, *41*, 13609−13619. (b) Kajiwara, T.; Nakano, M.; Takahashi, K.; Takaishi, S.; Yamashita, M. *Chem.—Eur. J.* **2011**, *17*, 196−205. (c) Mereacre, V.; Akhtar, M. N.; Lan, Y.; Ako, A. M.; Clérac, R.; Anson, C. E.; Powell, A. K. *Dalton Trans.* **2010**, *39*, 4918−4927.

(22) Jiang, S. D.; Wang, B. W.; Sun, H. L.; Wang, Z. M.; Gao, S. *J. Am. Chem. Soc.* **2011**, *133*, 4730−4733.

(23) Boulon, M. E.; Cucinotta, G.; Liu, S. S.; Jiang, S. D.; Ungur, L.; Chibotaru, L. F.; Gao, S.; Sessoli, R. *Chem.—Eur. J.* **2013**, *19*, 13726−13731.

(24) (a) Duncan, J. A. *J. Am. Chem. Soc.* **2009**, *131*, 2416−2416. (b) Aquilante, F.; De Vico, L.; Ferre, N.; Ghigo, G.; Malmqvist, P. A.; Neogrady, P.; Pedersen, T. B.; Pitonak, M.; Reiher, M.; Roos, B. O.; Serrano-Andres, L.; Urban, M.; Veryazov, V.; Lindh, R. *J. Comput. Chem.* **2010**, *31*, 224−247. (c) Veryazov, V.; Widmark, P. O.; Serrano-Andres, L.; Lindh, R.; Roos, B. O. *Int. J. Quantum Chem.* **2004**, *100*, 626−635. (d) Karlstrom, G.; Lindh, R.; Malmqvist, P. A.; Roos, B. O.; Ryde, U.; Veryazov, V.; Widmark, P. O.; Cossi, M.; Schimmelpfennig, B.; Neogrady, P.; Seijo, L. *Comput. Mater. Sci.* **2003**, *28*, 222−239.

(25) Roos, B. O.; Lindh, R.; Malmqvist, P. A.; Veryazov, V.; Widmark, P. O.; Borin, A. C. *J. Phys.Chem. A* **2008**, *112*, 11431−11435.

(26) Malmqvist, P. A.; Roos, B. O.; Schimmelpfennig, B. *Chem. Phys. Lett.* **2002**, *357*, 230−240.

(27) Chibotaru, L. F.; Ungur, L. *J. Chem. Phys.* **2012**, *137*, 064112−64112.

(28) (a) Langley, S. K.; Ungur, L.; Chilton, N. F.; Moubaraki, B.; Chibotaru, L. F.; Murray, K. S. *Inorg. Chem.* **2014**, *53*, 4303−4315. (b) Habib, F.; Luca, O. R.; Vieru, V.; Shiddiq, M.; Korobkov, I.; Gorelsky, S. I.; Takase, M. K.; Chibotaru, L. F.; Hill, S.; Crabtree, R. H.; Murugesu, M. *Angew. Chem., Int. Ed.* **2013**, *52*, 11290−11293.

(29) Frisch, M. J.; Trucks, G. W.; Schlegel, H. B.; Scuseria, G. E.; Robb, M. A.; Cheeseman, J. R.; Scalmani, G.; Barone, V.; Mennucci, B.; Petersson, G. A.; Nakatsuji, H.; Caricato, M.; Li, X.; Hratchian, H. P.; Izmaylov, A. F.; Bloino, J.; Zheng, G.; Sonnenberg, J. L.; Hada, M.; Ehara, M.; Toyota, K.; Fukuda, R.; Hasegawa, J.; Ishida, M.; Nakajima, T.; Honda, Y.; Kitao, O.; Nakai, H.; Vreven, T.; Montgomery, J. A., Jr.; Peralta, J. E.; Ogliaro, F.; Bearpark, M.; Heyd, J. J.; Brothers, E.; Kudin, K. N.; Staroverov, V. N.; Kobayashi, R.; Normand, J.; Raghavachari, K.; Rendell, A.; Burant, J. C.; Iyengar, S. S.; Tomasi, J.; Cossi, M.; Rega, N.; Millam, N. J.; Klene, M.; Knox, J. E.; Cross, J. B.; Bakken, V.; Adamo, C.; Jaramillo, J.; Gomperts, R.; Stratmann, R. E.; Yazyev, O.; Austin, A. J.; Cammi, R.; Pomelli, C.; Ochterski, J. W.; Martin, R. L.; Morokuma, K.; Zakrzewski, V. G.; Voth, G. A.; Salvador, P.; Dannenberg, J. J.; Dapprich, S.; Daniels, A. D.; Farkas, Ö.; Foresman, J. B.; Ortiz, J. V.; Cioslowski, J.; Fox, D. J. *Gaussian 09*; Gaussian, Inc.: Wallingford, CT, 2009.

(30) (a) Stephens, P. J.; Devlin, F. J.; Chabalowski, C. F.; Frisch, M. J. *J. Phys. Chem.* **1994**, *98*, 11623−11627. (b) Becke, A. D. *J. Chem. Phys.* **1993**, *98*, 5648−5652. (c) Lee, C. T.; Yang, W. T.; Parr, R. G. *Phys. Rev. B* **1988**, *37*, 785−789. (d) Becke, A. D. *Phys. Rev. A* **1988**, *38*, 3098−3100.

(31) Cundari, T. R.; Stevens, W. J. *J. Chem. Phys.* **1993**, *98*, 5555−5565.

(32) Schafer, A.; Huber, C.; Ahlrichs, R. *J. Chem. Phys.* **1994**, *100*, 5829−5835.

(33) Runge, E.; Gross, E. K. U. *Phys. Rev. Lett.* **1984**, *52*, 997−1000.

(34) Neese, F. *WIREs Comput. Mol. Sci.* **2012**, *2*, 73−78.

(35) Klamt, A.; Schuurmann, G. *J. Chem. Soc., Perkin Trans. 2* **1993**, 799−805.

(36) (a) Chilton, N. F.; Collison, D.; McInnes, E. J. L.; Winpenny, R. E. P.; Soncini, A. *Nature Commun.* **2013**, *4*, Article No. 2551 (DOI: 10.1038/Ncomms3551). (b) Aravena, D.; Ruiz, E. *Inorg. Chem.* **2013**, *52*, 13770−13778.

(37) (a) Ishikawa, N.; Sugita, M.; Ishikawa, T.; Koshihara, S.; Kaizu, Y. *J. Phys. Chem. B* **2004**, *108*, 11265−11271. (b) Abragam, A.; Bleaney, B. *Electron Paramagnetic Resonance of Transition Ions*; Dover Publications: Dover, NY, 1986.

(38) Note: (a) Orbach process is a type of spin-lattice relaxation and depends on the splitting pattern of the three involved states. The rate for this process vanishes for $T \rightarrow 0$ K exponentially.. (b) Raman process is a type of two-phonon direct spin-lattice relaxation mechanism, where the spin system is under non-adiabatic conditions. Such analysis permits us to make a detailed study of this process, including the case of multilevel ground states (S-electron ions with hyperfine interaction), as well as the case of the sharp resonant modes associated with the paramagnetic impurities..

(39) Ungur, L.; Thewissen, M.; Costes, J.-P.; Wernsdorfer, W.; Chibotaru, L. F. *Inorg. Chem.* **2013**, *52*, 6328−6337.

(40) Schrefl, T.; Fidler, J.; Suess, D.; Scholz, W.; Tsiantos, V. In *Micromagnetic Simulation of Dynamic and Thermal Effects*; Institute of Applied and Technical Physics, Vienna University of Technology, Wien, Germany.

(41) Ğorller-Walrand, C.; Gschneidner, K. A., Jr.; Eyring, L. In *Handbook on the Physics and Chemistry of Rare Earths*, Vol. *23*; North−Holland: Amsterdam, 1996.

(42) Note: It is important to note here that Raman and Orbach processes cannot be directly determined by these matrix elements. These matrix elements can be useful as the indicator toward these processes.

(43) Konig, S. N.; Chilton, N. F.; Maichle-Mossmer, C.; Pineda, E. M.; Pugh, T.; Anwander, R.; Layfield, R. A. *Dalton Trans.* **2014**, *43*, 3035−3038.

(44) Note: (a) studied models are fictitious and not optimized structures, thus the Er-O-H angles are expected to be non-linear. Other possible linear arrangements are Er-C-N moiety which are also reported in the literature.. (b) Jank, S.; Guttenberger, C.; Reddmann, H.; Hanss, J.; Amberger, H. D. *Z. Anorg. Allg. Chem.* **2006**, *632*, 2429−2438. (c) Chen, W. T.; Wu, A. Q.; Guo, G. C.; Wang, M. S.; Cai, L. Z.; Huang, J. S. *Eur. J. Inorg. Chem.* **2010**, 2826−2835. (d) Tian, Y. P.; Li, L.; Zhou, Y. H.; Wang, P.; Zhou, H. P.; Wu, J. Y.; Hu, Z. J.; Yang, J. X.; Kong, L.; Xu, G. B.; Tao, X. T.; Jiang, M. H. *Cryst. Growth Des.* **2009**, *9*, 1499−1504. (e) de Oliveira, G. M.; Machado, A.; Gomes, G. W.; Monteiro, J. H. S. K.; Davolos, M. R.; Abram, U.; Jagst, A. *Polyhedron* **2011**, *30*, 851−859.

(45) (a) Herrmann, W. A.; Anwander, R.; Munck, F. C.; Scherer, W.; Dufaud, V.; Huber, N. W.; Artus, G. R. J. *Z. Naturforsch., B: Chem. Sci.* **1994**, *49*, 1789−1797. (b) Bradley, D. C.; Ghotra, J. S.; Hart, F. A. *J. Chem. Soc.,Chem. Commun.* **1972**, 349−350.
(46) Zhang, P.; Zhang, L.; Wang, C.; Xue, S.; Lin, S.-Y.; Tang, J. *J. Am. Chem. Soc.* **2014**, *136*, 4484−4487.
(47) Boulon, M.-E.; Cucinotta, G.; Luzon, J.; Degl'Innocenti, C.; Perfetti, M.; Bernot, K.; Calvez, G.; Caneschi, A.; Sessoli, R. *Angew. Chem., Int. Ed.* **2013**, *52*, 350−354.
(48) Le Roy, J. J.; Ungur, L.; Korobkov, I.; Chibotaru, L. F.; Murugesu, M. *J. Am. Chem. Soc.* **2014**, *136*, 8003−8010.
(49) Ungur, L.; Le Roy, J. J.; Korobkov, I.; Murugesu, M.; Chibotaru, L. F. *Angew. Chem., Int. Ed.* **2014**, *53*, 4413−4417.
(50) Le Roy, J. J.; Jeletic, M.; Gorelsky, S. I.; Korobkov, I.; Ungur, L.; Chibotaru, L. F.; Murugesu, M. *J. Am. Chem. Soc.* **2013**, *135*, 3502−3510.
(51) Langley, S. K.; Wielechowski, D. P.; Vieru, V.; Chilton, N. F.; Moubaraki, B.; Chibotaru, L. F.; Murray, K. S. *Chem. Sci.* **2014**, *5*, 3246−3256.